Meccanica **33:** 229–242, 1998.

Postcritical Behavior of Cables Undergoing Two Simultaneous Galloping Modes

ANGELO LUONGO[1], ACHILLE PAOLONE[1] and GIUSEPPE PICCARDO[2]
[1]*University of L'Aquila, Dipartimento di Ingegneria delle Strutture, delle Acque e del Terreno, DISAT; 67040 Monteluco di Roio (L'Aquila), Italy*
[2]*University of Genoa, Dipartimento di Ingegneria Strutturale e Geotecnica, DISEG Via Montallegro 1; 16145 Genoa, Italy*

(Received: 30 March 1997; accepted in final form: 30 January 1998)

Abstract. A nonlinear two degree-of-freedom model, describing a flexible elastic suspended cable undergoing galloping oscillations, is analyzed. By using a perturbative approach, the critical conditions occuring for different values of the aerodynamic coefficients are described. Two different type of critical conditions, corresponding to simple or double Hopf bifurcations are found. The nonlinear postcritical behavior of single taut strings in 1:1 primary internal resonance is studied through the multiple scale perturbation method. In the double Hopf bifurcation case the influence of the detuning between the critical eigenvalues on the postcritical behavior is illustrated. It is found that quasi-periodic motions, which are likely to occur in the linear field when the two critical frequencies are incommensurable, are really unstable in the nonlinear range. Therefore, the postcritical behavior of the string consists of stable periodic motions for any detuning values.

Sommario. Viene analizzato un modello non lineare a due gradi di libertà, rappresentativo di un cavo elastico flessibile sospeso alle estremità e soggetto ad oscillazioni galoppanti. Utilizzando un approccio perturbativo, vengono descritte le condizioni critiche per differenti valori dei coefficienti aerodinamici. Sono presenti due diversi tipi di condizioni critiche, corrispondenti a biforcazioni di Hopf semplici e doppie. Attraverso il metodo perturbativo delle scale multiple viene studiato il comportamento post-critico non lineare di singole stringhe tese in risonanza interna primaria 1:1. Nel caso di biforcazione doppia di Hopf viene illustrata l'influenza del detuning tra gli autovalori critici sul comportamento post-critico. Si trova che i moti quasi-periodici, presenti in campo lineare quando le due frequenze critiche sono incommensurabili, sono in realtà instabili in campo non lineare. Quindi, il comportamento post-critico della stringa risulta composto da moti periodici stabili per un qualsiasi valore del detuning.

Key words: Galloping, Perturbation methods, Cables, Wind engineering, Structural dynamics.

1. Introduction

Transmission lines subject to icing conditions must be designed with large clearances to prevent clashing and possible power failures as they can experience self-excited aeroelastic oscillations of large amplitude due to wind, predominantly in the vertical plane, called galloping. The problem has been studied in the literature for slender beams or taut strings, both in linear and nonlinear fields, using simple models with one or two d.o.f. (e.g. [1]). Large galloping oscillations of suspended cables have only recently been analyzed for a three d.o.f. system [2]. In these works, however, only the aerodynamic nonlinearities have been taken into account, while geometric nonlinearities have been ignored. The latter, on the contrary, play an important role in describing the dynamic behavior of cables, as already highlighted in many works on the subject (e.g. [3, 4]). Therefore, to correctly describe the nonlinear galloping of iced suspended

cables it is necessary to formulate a consistent mechanical model accounting for both types of nonlinearity, as presented in [5]. In that paper, coupled in-plane and out-of-plane motions of a flexible elastic suspended cable in internal resonance conditions of 1:2 type have been analyzed, and the nonlinear postcritical behavior around a simple Hopf bifurcation has been studied.

However, the simple Hopf bifurcation is not the only instability form experienced by cables subject to wind. In fact, in [6] it has been shown that when the in-plane and out-of-plane fundamental frequencies of the cable coincide, two qualitatively different critical conditions occur for different values of the aerodynamic coefficients, called 'galloping' and 'complex galloping', the latter characterized by beating motion. In this way the Den Hartog criterion (valid for in-plane galloping) is extended to take into account the intrinsic coupling between in-plane and out-of-plane motion. These results have been generalized in [7], where detuned frequencies have been considered too, and a perturbative approach has been used, leading to simpler analytical expressions. It has been pointed out that, the true characteristic of 'complex galloping' is not the complexity (which, on the contrary, is common in galloping as regards eigensolutions), but the existence of two couples of critical eigenvalues (i.e. double Hopf bifurcation), whereas the usual galloping critical condition is a simple Hopf bifurcation. This new type of critical condition is potentially very dangerous and can be responsible for possible bi-modal galloping and quasi-periodic motions. In neither papers, [6] and [7], has the complete scenario of the critical conditions in the parameter space been furnished. Moreover, only the linear bifurcation problem has been dealt with, so that no information is available on the postcritical behavior of the cable. In particular the existence of quasi-periodic motions predicted from the linear theory has not been checked in the nonlinear field.

In this paper both items are addressed: (1) to present the scenario of the critical conditions and to discuss their codimension; (2) to analyze the local postcritical behavior of the cable, by focusing the attention on the existence and stability of coupled, two-mode solutions. The continuous model presented in [5] is considered again. Here, attention is focused on taut strings for which 1:1 internal resonance occur. After discretization and use of the multiple scale perturbation method, amplitude and phase equations are obtained. Steady-state amplitude solutions are determined as a function of the non-dimensional mean wind speed, assumed as the control parameter. For a wind speed over critical value, phase curves are obtained by numerical integrations of the amplitude modulation equations; the stability and the attraction basins of the fixed points are analyzed.

2. Model

Let us consider a flexible heavy hyperelastic cable suspended between two fixed supports. Referring to the Frenet triad, in which the aerodynamic forces are more easily expressed, the non-dimensional equations that govern the prevalently transversal motion of the cable in the small curvature regime are [4, 8]:

$$\begin{aligned} &[1+\alpha e]u_1'' + f_1 = \pi^2 \ddot{u}_1 \\ &[1+\alpha e]u_2'' + \alpha\beta e + f_2 = \pi^2 \ddot{u}_2, \quad u_i(0,t) = u_i(1,t) = 0 \end{aligned} \tag{1}$$

where

$$e = u_3' - \beta u_2 + \tfrac{1}{2}(u_2'^2 + u_1'^2) \tag{2}$$

is the dynamic component of the Lagrangian strain when the curvature is small, which is (approximately) constant along the cable. The following non-dimensional quantities are used in

equations (1) and (2):

$$u_i = \frac{U_i}{L}, \quad s = \frac{S}{L}, \quad f_i = \frac{L}{H} F_i, \quad t = \frac{\pi}{L}\sqrt{\frac{H}{m}}T,$$
$$\alpha = \frac{EA}{H}, \quad \beta \approx \frac{8d}{L}, \quad \mu = \frac{\rho b V}{m}\sqrt{\frac{L}{g}} \tag{3}$$

where u_i are the out-of-plane ($i = 1$) and in-plane ($i = 2$) displacement components measured from the static equilibrium configuration; f_i are distributed dynamic force components due to wind, depending on velocities $\dot{u}_i$ and on the non-dimensional mean wind speed μ; m is the mass per unity length of the cable (ice included); g is the acceleration due to gravity; L is the cable length; H is the horizontal component of static tension; EA is the axial stiffness; d is the cable sag at mid-span. Dots and apices denote derivatives with respect to the non-dimensional time t and curvilinear abscissa s, respectively. Torsional effects are neglected since single cables usually have torsional frequency much higher than two flexural frequencies [9]. The aerodynamic forces f_i are determined with reference to a spring-mounted damped rigid cylinder of indefinite length, subjected to a bidimensional turbulent flow of uniform velocity V, in the quasi-static regime (i.e. at much lower oscillation frequencies than the vortex-shedding frequency).

By applying the Galerkin method and using the first in-plane and out-of-plane eigenfunction of the linearized problem, a discrete model is obtained [5]:

$$\ddot{q}_1 + b_1\dot{q}_1 + b_2\dot{q}_2 + \omega_1^2 q_1 + c_1 q_1 q_2 + c_2 q_1^3 + c_3 q_1 q_2^2 + b_5\dot{q}_1^2 + b_6\dot{q}_2^2 + b_7\dot{q}_1\dot{q}_2 + b_8\dot{q}_2^3 = 0 \tag{4}$$

$$\ddot{q}_2 + b_3\dot{q}_1 + b_4\dot{q}_2 + \omega_2^2 q_2 + c_4 q_1^2 + c_5 q_2^2 + c_6 q_1^2 q_2 + c_7 q_2^3 + b_9\dot{q}_1^2 + b_{10}\dot{q}_2^2 + b_{11}\dot{q}_1\dot{q}_2 + b_{12}\dot{q}_2^3 = 0, \tag{5}$$

where $q_i(t)$ describe the temporal behavior of the out-of-plane ($i=1$) and in-plane ($i=2$) degree-of-freedom; ω_i are the Hamiltonian non-dimensional natural frequencies; b_i are coefficients of linear and nonlinear aerodynamic forces depending on μ; c_i are coefficients of nonlinear geometric terms; constant forces, driven by the mean wind speed, are neglected likewise in [6, 7]. The expressions of coefficients b_i and c_i are given in Appendix A. By focusing attention on simple taut strings, the Hamiltonian frequencies are coincident, $\omega_1=\omega_2=\omega$, and the mechanical quadratic coefficients are equal to zero ($c_1=c_4=c_5=0$) while aerodynamic quadratic coefficients ($b_5, b_6, b_7, b_9, b_{10}, b_{11}$) are still different from zero. Equations (1), (4) and (5) admit the trivial solution $u_i = 0$ and $q_i = 0$, respectively, for any value of the mean wind speed μ.

3. Critical Conditions Scenario

The first step of the analysis concerns the study of the critical conditions. It requires evaluation of the eigenvalues of the linear part of the discretized equations (4) and (5). In [7], by assuming that all damping coefficients b_i are small of the same order and applying a perturbative method, an approximate expression for the eigenvalues is obtained in the more general case of slightly

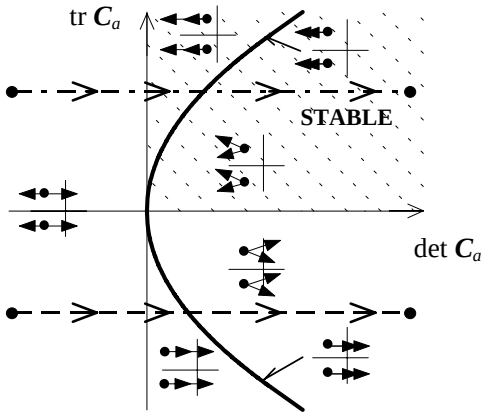

Figure 1. Critical conditions in the plane of aerodynamic damping matrix invariants.

detuned frequencies. In particular, for taut strings, they read:

$$\lambda_{1,2} = \pm i\omega - \frac{b_1 + b_4}{4} + \frac{1}{4}\sqrt{(b_1 - b_4)^2 + 4b_2 b_3},$$
$$\lambda_{3,4} = \pm i\omega - \frac{b_1 + b_4}{4} - \frac{1}{4}\sqrt{(b_1 - b_4)^2 + 4b_2 b_3}. \tag{6}$$

Here, starting from equations (6), the galloping critical condition scenario is built up. By separating the total damping matrix $\mathbf{C}$ in its structural $\mathbf{C}_\mathrm{s}$ and aerodynamic $\mathbf{C}_\mathrm{a}$ components and assuming structural damping coefficient equal in both directions (i.e. $\mathbf{C} = \mathbf{C}_\mathrm{s} + \mu\mathbf{C}_\mathrm{a}$, $\mathbf{C}_\mathrm{s} = 2\omega\,\mathrm{diag}\,\{\xi\}$), equations (6) are rewritten in the following expressive way:

$$\lambda_{1,2} = \pm i\omega - \omega\xi - \frac{\mu}{4}(\mathrm{tr}\mathbf{C}_\mathrm{a} - \sqrt{(\mathrm{tr}\mathbf{C}_\mathrm{a})^2 - 4\,\mathrm{det}\mathbf{C}_\mathrm{a}}) = \alpha_1 + i\,(\beta_1 \pm \omega)$$
$$\lambda_{3,4} = \pm i\omega - \omega\xi - \frac{\mu}{4}(\mathrm{tr}\mathbf{C}_\mathrm{a} + \sqrt{(\mathrm{tr}\mathbf{C}_\mathrm{a})^2 - 4\,\mathrm{det}\mathbf{C}_\mathrm{a}}) = \alpha_2 + i(\beta_2 \pm \omega), \tag{7}$$

where i is the imaginary unity, and $\mathrm{tr}\mathbf{C}_\mathrm{a}$ and $\mathrm{det}\mathbf{C}_\mathrm{a}$ are respectively the trace and the determinant of the aerodynamic damping matrix $\mathbf{C}_\mathrm{a}$. It can be checked that the critical conditions $\alpha_i = 0$ $(i = 1, 2)$ furnished by equations (7) coincide with the exact conditions given in [6]. Moreover, if $\beta_i = 0$ (radical quantity positive) the critical modes are real, whereas if $\beta_i \neq 0$ (radical quantity negative) two complex critical modes exist with non-nil components on both degrees of freedom.

The scenario is represented in the plane of the invariants $(\mathrm{det}\mathbf{C}_\mathrm{a}, \mathrm{tr}\mathbf{C}_\mathrm{a})$, where the paths of the eigenvalues on the complex plane, when the mean wind speed μ is increased from zero, are illustrated for each region. The presence of a region of possible double Hopf bifurcations, bounded in the fourth quadrant by the horizontal axis and the parabola, takes on particular interest. The figure is discussed for different values of the determinant of the aerodynamic damping matrix, keeping the trace constant, that is by considering a class of iced cables with different aerodynamic properties (e.g. different ice shapes). There are two main cases, depending on the sign of the trace. For negative trace, going from left to right (dashed line in Figure 1), different bifurcation mechanisms exist. At first, in the third quadrant, a simple Hopf bifurcation occurs. As soon as the vertical axis is passed through, two couples of eigenvalues cross the imaginary axis but in a non-simultaneous way. On the parabola, a double Hopf bifurcation occurs

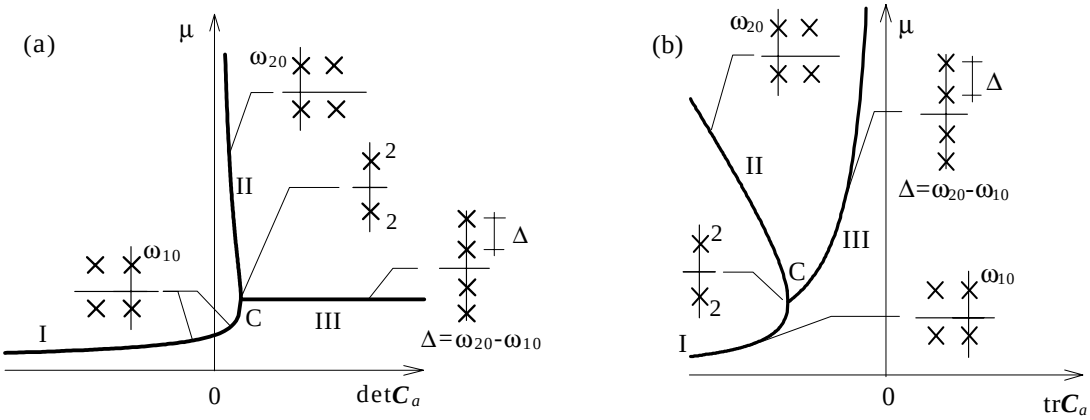

Figure 2. Stability boundaries: (a) $(\mu, \det\mathbf{C}_a)$-plane, $\mathrm{tr}\mathbf{C}_a < 0$; (b) $(\mu, \mathrm{tr}\mathbf{C}_a)$-plane, $\det\mathbf{C}_a > 0$.

with coincident critical eigenvalues. In this limit case the detuning $\Delta := |\beta_2 - \beta_1| \equiv \omega_{20} - \omega_{10}$ between the couples of critical eigenvalues is equal to zero. Here a defective situation occurs, in which the geometric multiplicity of the critical eigenvalue is less than its algebraic multiplicity. Finally, when the parabola is passed, double Hopf bifurcations occur with a non-vanishing detuning Δ, which progressively increases to the right. When the trace is positive, going from left to right (dot-dashed line in Figure 1), only a simple Hopf bifurcation is encountered for negative determinant, while the system is always stable in the first quadrant.

In order to perform a postcritical nonlinear analysis, it is necessary to identify the control parameters correctly. Equations (7) point out that the eigenvalues real part α_i depends on μ, $\mathrm{tr}\mathbf{C}_a$ and $\det\mathbf{C}_a$; hence, it appears that control parameters have to be selected from among them. The stability boundaries related to the three parameters are shown in Figure 2, for fixed values of trace (Figure 2(a)) or determinant (Figure 2(b)). Along branches I and II a simple Hopf bifurcation occurs ($\alpha_1 = 0$ or $\alpha_2 = 0$ respectively); along branch III a double Hopf bifurcation manifests itself ($\alpha_1 = \alpha_2 = 0$). Therefore there exists a line in $\Re^2$ Euclidean space (or a surface in $\Re^3$ space) representing the locus of both single and double Hopf bifurcations. With regard to this latter, in a generic case in which the critical frequencies are in a non-integer ratio (i.e. in a non-resonant condition), the bifurcation is described by a single parameter, that is, *the problem has codimension one*. This is very unusual for double Hopf bifurcations which generally have codimension two (e.g. [10, 11]). Here, a non-generic case for a single parameter is represented by the point C ($\Delta = 0$, Figure 2), which corresponds to a defective bifurcation having codimension two. In this paper point C will not be studied, since the relevant analysis requires employing a special technique. However, a neighborhood of C is tentatively studied (nearly-resonant condition) by assuming that, sufficiently far from C, the two eigenvectors are linearly independent (non-defective case) while the associated eigenvalues are still close to each other. In fact the eigenvectors of weakly damped Hamiltonian systems (as those presented here) exhibit marked sensitivity in a small neighborhood of the defective system, whereas the eigenvalues are moderately sensitive [12]. Thus, the actual system is considered as a Δ-perturbation of an ideal non-defective resonant system.

In the non-resonant case, the more significant control parameter appears to be the non-dimensional mean wind speed μ; in the nearly-resonant case, the detuning Δ (depending both on $\mathrm{tr}\mathbf{C}_a$ and $\det\mathbf{C}_a$) has to be added as second control parameter.

4. Nonlinear Analysis

The equation of motion (4, 5) are written in the first-order local form as follows:

$$\dot{\mathbf{x}} = \mathbf{F}(\mathbf{x}, \nu) \tag{8}$$

in which $\mathbf{x}(t) = \{\dot{q}_1, \dot{q}_2, q_1, q_2\}^T$ and $\nu := \mu - \mu_c$ is the new control parameter, where μ_c corresponds to a critical condition. A second control parameter will be introduced later in the nearly-resonant case.

Equation (8) admits the trivial equilibrium solution consisting of the set of states $\Gamma := \{(\mathbf{x}, \nu)|\mathbf{x} = \mathbf{0}\}$. At $\mathbf{O} \equiv (\mathbf{x} = \mathbf{0}, \nu = 0)$ it undergoes a single or double Hopf bifurcation. Equation (8) is solved around the bifurcation point $\mathbf{O}$ by using the multiple scale method (*MSM*), by looking for a family of monoparametric solutions of the form:

$$\mathbf{x} = \mathbf{x}(\varepsilon, t_0, t_2, \dots), \quad \nu = \nu(\varepsilon), \tag{9}$$

where $t_0 = t, t_2 = (\varepsilon^2/2!)t, \dots, t_{2k} = [\varepsilon^{2k}/(2k)!]t$ are independent temporal scales.

Under hypotheses of regularity, equations (9) are expressed in Mac Laurin series:

$$\mathbf{x} = \sum_{k=1}^{\infty} \frac{\varepsilon^k}{k!}\,\mathbf{x}_k, \qquad \nu = \sum_{k=2,4,\dots,}^{\infty} \frac{\varepsilon^k}{k!}\,\nu_k, \tag{10}$$

where $\mathbf{x}_k = \mathbf{x}_k(t_0, t_2, \dots)$, and $\varepsilon = 0$ selects the bifurcation point. The time derivative is expressed as:

$$\frac{\mathrm{d}}{\mathrm{d}t} = \mathrm{d}_0 + \frac{\varepsilon^2}{2!}\,\mathrm{d}_2 + \cdots + \frac{\varepsilon^{2k}}{2k!}\,\mathrm{d}_{2k} + \cdots, \tag{11}$$

where $\mathrm{d}_k = \partial/\partial t_k$. By differentiating k times equation (8) with respect to the parameter ε and evaluating the derivatives at $\varepsilon = 0$, the perturbative equations of k-order are obtained. For $k = 1, 2, 3$, by using equations (10) and (11), they read:

$$(\mathrm{d}_0\mathbf{E} - \mathbf{F}^0_{\mathbf{x}})\mathbf{x}_1 = \mathbf{0}, \tag{12}$$

$$(\mathrm{d}_0\mathbf{E} - \mathbf{F}^0_{\mathbf{x}})\mathbf{x}_2 = \mathbf{F}^0_{\mathbf{xx}}\mathbf{x}_1^2, \tag{13}$$

$$(\mathrm{d}_0\mathbf{E} - \mathbf{F}^0_{\mathbf{x}})\mathbf{x}_3 = 3\nu_2\mathbf{F}^0_{\mathbf{x}\nu}\mathbf{x}_1 + 3\mathbf{F}^0_{\mathbf{xx}}\mathbf{x}_1\mathbf{x}_2 + \mathbf{F}^0_{\mathbf{xxx}}\mathbf{x}_1^3 - 3\mathrm{d}_2\mathbf{x}_1, \tag{14}$$

where $\mathbf{E}$ is the 4×4 identity matrix, the subscripts $(\mathbf{x}, \nu)$ denote partial differentiation and the apex 0 indicates that the related quantity is calculated at $\varepsilon = 0$.

With reference to a double Hopf bifurcation, depending on the magnitude of the detuning Δ at the critical point, two cases are analyzed: (a) $\Delta \cong 0$ (nearly-resonant case) or (b) $\Delta = \mathrm{O}(1)$ (non-resonant case). They correspond to critical conditions (a) near or (b) far from to the double Hopf bifurcation boundaries, represented in Figure 1 by the parabola. In both cases the generating solution of equation (12) is given by:

$$\mathbf{x}_1 = A_1(t_2, t_4, \dots)\mathbf{u}_1 e^{i\omega_{10}t_0} + A_2(t_2, t_4, \dots)\mathbf{u}_2 e^{i\omega_{20}t_0} + c.c., \tag{15}$$

where the functions A_j are undetermined at this level and $\mathbf{u}_j$ are the right eigenvectors of the Jacobian matrix $\mathbf{F}^0_{\mathbf{x}}$ associated with the critical eigenvalues ω_{j0} (Figure 2).

Substituting the first-order solution given by equation (15) into equation (13) yields:

$$\begin{aligned}(\mathrm{d}_0\mathbf{E}-\mathbf{F}^0_{\mathbf{x}})\mathbf{x}_2 \;=\;& A_1^2\mathbf{F}^0_{\mathbf{xx}}\mathbf{u}_1^2\,e^{i2\omega_{10}t_0}+A_2^2\mathbf{F}^0_{\mathbf{xx}}\mathbf{u}_2^2\,e^{i2\omega_{20}t_0}+\\ &+2A_1A_2\mathbf{F}^0_{\mathbf{xx}}\mathbf{u}_1\mathbf{u}_2\,e^{i(\omega_{10}+\omega_{20})t_0}+A_1\bar{A}_1\mathbf{F}^0_{\mathbf{xx}}\mathbf{u}_1\bar{\mathbf{u}}_1+\\ &+A_2\bar{A}_2\mathbf{F}^0_{\mathbf{xx}}\mathbf{u}_2\bar{\mathbf{u}}_2+2A_1\bar{A}_2\mathbf{F}^0_{\mathbf{xx}}\mathbf{u}_1\bar{\mathbf{u}}_2\,e^{i(\omega_{10}-\omega_{20})t_0}+c.c.\end{aligned}\tag{16}$$

If the one-to-two internal resonance is excluded, all terms on the right-hand side of equation (16) are non-resonant; therefore the solution of equation (16) is:

$$\begin{aligned}\mathbf{x}_2 =\;& A_1^2\mathbf{z}_{11}e^{i2\omega_{10}t_0}+A_2^2\mathbf{z}_{22}e^{i2\omega_{20}t_0}+2A_1A_2\mathbf{z}_{12}e^{i(\omega_{10}+\omega_{20})t_0}+\\ &+A_1\bar{A}_1\mathbf{z}_{1\bar{1}}+A_2\bar{A}_2\mathbf{z}_{2\bar{2}}+2A_1\bar{A}_2\mathbf{z}_{1\bar{2}}e^{i(\omega_{10}-\omega_{20})t_0}+c.c.,\end{aligned}\tag{17}$$

where the $\mathbf{z}_{rs}$'s and $\mathbf{z}_{r\bar{s}}$'s ($r, s = 1, 2$) are solutions of the non-singular algebraic problems:

$$\begin{aligned}[i(p\omega_{10}+q\omega_{20})\,\mathbf{E}-\mathbf{F}^0_{\mathbf{x}}]\mathbf{z}_{rs} \;&=\; \mathbf{F}^0_{\mathbf{xx}}\mathbf{u}_r\mathbf{u}_s\\ [i(p\omega_{10}-q\omega_{20})\,\mathbf{E}-\mathbf{F}^0_{\mathbf{x}}]\mathbf{z}_{r\bar{s}} \;&=\; \mathbf{F}^0_{\mathbf{xx}}\mathbf{u}_r\bar{\mathbf{u}}_s\end{aligned}\tag{18}$$

being p and q the coefficients of ω_{10} and ω_{20}, respectively, which appear in equation (17) in the associated exponential functions. Moreover, the following properties hold: $\mathbf{z}_{rs}=\mathbf{z}_{sr}$, $\bar{\mathbf{z}}_{r\bar{s}}=\mathbf{z}_{\bar{r}s}$.

Substituting equations (15) and (17) into equations (14), it follows:

$$\begin{aligned}\left(\mathrm{d}_0\mathbf{E}-\mathbf{F}^0_{\mathbf{x}}\right)\mathbf{x}_3 \;=\;& 3\left\{\nu_2A_1\mathbf{F}^0_{\mathbf{x}\nu}\mathbf{u}_1+A_1^2\bar{A}_1\left[\mathbf{F}^0_{\mathbf{xx}}\left(2\mathbf{u}_1\mathbf{z}_{1\bar{1}}+\mathbf{z}_{11}\bar{\mathbf{u}}_1\right)+\mathbf{F}^0_{\mathbf{xxx}}\mathbf{u}_1^2\bar{\mathbf{u}}_1\right]+\right.\\ &+2A_1A_2\bar{A}_2\left[\mathbf{F}^0_{\mathbf{xx}}\left(\mathbf{u}_1\mathbf{z}_{2\bar{2}}+\mathbf{u}_2\mathbf{z}_{1\bar{2}}+\mathbf{z}_{12}\bar{\mathbf{u}}_2\right)+\mathbf{F}^0_{\mathbf{xxx}}\mathbf{u}_1\mathbf{u}_2\bar{\mathbf{u}}_2\right]-\\ &\left.-\;\mathrm{d}_2A_1\mathbf{u}_1\right\}e^{i\omega_{10}t_0}+\\ &+3\left\{\nu_2A_2\mathbf{F}^0_{\mathbf{x}\nu}\mathbf{u}_2+A_2^2\bar{A}_2\left[\mathbf{F}^0_{\mathbf{xx}}\left(2\mathbf{u}_2\mathbf{z}_{2\bar{2}}+\mathbf{z}_{22}\bar{\mathbf{u}}_2\right)+\mathbf{F}^0_{\mathbf{xxx}}\mathbf{u}_2^2\bar{\mathbf{u}}_2\right]+\right.\\ &+2A_2A_1\bar{A}_1\left[\mathbf{F}^0_{\mathbf{xx}}\left(\mathbf{u}_2\mathbf{z}_{1\bar{1}}+\mathbf{u}_1\mathbf{z}_{\bar{1}2}+\mathbf{z}_{12}\bar{\mathbf{u}}_1\right)+\mathbf{F}^0_{\mathbf{xxx}}\mathbf{u}_1\bar{\mathbf{u}}_1\mathbf{u}_2\right]-\\ &\left.-\;\mathrm{d}_2A_2\mathbf{u}_2\right\}e^{i\omega_{20}t_0}+\\ &+3A_1^2\bar{A}_2\left[\mathbf{F}^0_{\mathbf{xx}}\left(2\mathbf{u}_1\mathbf{z}_{1\bar{2}}+\bar{\mathbf{u}}_2\mathbf{z}_{11}\right)+\mathbf{F}^0_{\mathbf{xxx}}\mathbf{u}_1^2\bar{\mathbf{u}}_2\right]e^{i(2\omega_{10}-\omega_{20})t_0}+\\ &+3A_2^2\bar{A}_1\left[\mathbf{F}^0_{\mathbf{xx}}\left(2\mathbf{u}_2\mathbf{z}_{\bar{1}2}+\bar{\mathbf{u}}_1\mathbf{z}_{22}\right)+\mathbf{F}^0_{\mathbf{xxx}}\mathbf{u}_2^2\bar{\mathbf{u}}_1\right]e^{i(2\omega_{20}-\omega_{10})t_0}+\\ &+c.c.+N.S.T.\end{aligned}\tag{19}$$

Because the homogeneous part of equation (14) has a nontrivial solution the nonhomogeneous equation (19) has a solution only if a solvability condition is satisfied. This condition requires the right-hand side of equation (19) be orthogonal to every solution of the adjoint homogeneous problem.

First, the nearly-resonant case is dealt with. To express the nearness of ω_{20} to ω_{10}, the detuning:

$$\Delta=(\omega_{20}-\omega_{10})\,\varepsilon^{-2}\tag{20}$$

is introduced as a second parameter. Substituting equation (20) into equation (19) and eliminating the secular terms from equation (19), it follows:

$$\begin{aligned}\mathrm{d}_2A_1 \;=\;& C_{11}\nu_2A_1+8C_{12}A_1^2\bar{A}_1+8C_{13}A_1A_2\bar{A}_2+\\ &+(C_{14}\nu_2A_2+8C_{15}A_2^2\bar{A}_2+8C_{16}A_2A_1\overline{A}_1)e^{i\Delta t_2}+\\ &+8C_{17}A_1^2\bar{A}_2e^{-i\Delta t_2}+8C_{18}A_2^2\bar{A}_1e^{i2\Delta t_2}\end{aligned}\tag{21}$$

$$\begin{aligned} \mathrm{d}_2 A_2 \;=\; & (C_{21}\nu_2 A_1 + 8C_{22}A_1^2\bar{A}_1 + 8C_{23}A_1A_2\bar{A}_2)e^{-i\Delta t_2} + \\ & + C_{24}\nu_2 A_2 + 8C_{25}A_2^2\bar{A}_2 + 8C_{26}A_1A_2\bar{A}_1 + \\ & + 8C_{27}A_1^2\bar{A}_2 e^{-i2\Delta t_2} + 8C_{28}A_2^2\bar{A}_1 e^{i\Delta t_2}, \end{aligned} \tag{22}$$

where the coefficients C's are given in Appendix B. Expressing A_j in the polar form:

$$A_j = \tfrac{1}{2}a_j e^{i\varphi_j} \tag{23}$$

and separating equations (21) and (22) into real and imaginary parts, coming back to the real time t by means of equation (11) and reabsorbing the parameter ε, the following autonomous equation set is drawn:

$$\begin{aligned} \dot{a}_1 \;=\; & \nu R_{11}a_1 + R_{12}a_1^3 + R_{13}a_1a_2^2 + \\ & + (\nu R_{14}a_2 + R_{15}a_2^3 + R_{16}a_1^2a_2)\cos\gamma - (\nu I_{14}a_2 + I_{15}a_2^3 + I_{16}a_1^2a_2)\sin\gamma + \\ & + R_{17}a_1^2a_2\cos\gamma + R_{18}a_1a_2^2\cos 2\gamma + I_{17}a_1^2a_2\sin\gamma - I_{18}a_1a_2^2\sin 2\gamma \end{aligned} \tag{24}$$

$$\begin{aligned} \dot{a}_2 \;=\; & \nu R_{24}a_2 + R_{25}a_2^3 + R_{26}a_2a_1^2 + \\ & + (\nu R_{21}a_1 + R_{22}a_1^3 + R_{23}a_1a_2^2)\cos\gamma + (\nu I_{21}a_1 + I_{22}a_1^3 + I_{23}a_1a_2^2)\sin\gamma + \\ & + R_{28}a_1a_2^2\cos\gamma - a_1a_2^2I_{28}\sin\gamma + R_{27}a_1^2a_2\cos 2\gamma + I_{27}a_1^2a_2\sin 2\gamma \end{aligned} \tag{25}$$

$$\begin{aligned} a_1a_2\dot{\gamma} \;=\; & (\nu I_{21}a_1 + I_{22}a_1^3 + I_{23}a_1a_2^2)a_1\cos\gamma - \\ & - (\nu R_{21}a_1 + R_{22}a_1^3 + R_{23}a_1a_2^2)a_1\sin\gamma + \\ & + \nu I_{24}a_1a_2 + I_{25}a_1a_2^3 + I_{26}a_1^3a_2 + I_{27}a_1^3a_2\cos 2\gamma - R_{27}a_1^3a_2\sin 2\gamma - \\ & - a_2\left(\nu I_{11}a_1 + I_{12}a_1^3 + I_{13}a_1a_2^2\right) - \left(\nu I_{14}a_2 + I_{15}a_2^3 + I_{16}a_2a_1^2\right)a_2\cos\gamma - \\ & - (\nu R_{14}a_2 + R_{15}a_2^3 + R_{16}a_2a_1^2)a_2\sin\gamma + R_{28}a_2^2a_1^2\sin\gamma + I_{28}a_2^2a_1^2\cos\gamma - \\ & - I_{17}a_1^2a_2^2\cos\gamma + R_{17}a_1^2a_2^2\sin\gamma - I_{18}a_1a_2^3\cos 2\gamma - \\ & - R_{18}a_1a_2^3\sin 2\gamma + a_1a_2\Delta, \end{aligned} \tag{26}$$

where $\gamma := \varphi_2 - \varphi_1 + \Delta t$ is the phase difference and coefficient R's and I's are respectively the real and imaginary parts of the coefficient C's. The fixed points of the equations (24–26) are determined by setting $\dot{a}_1 = \dot{a}_2 = \dot{\gamma} = 0$. These solutions correspond to a one-frequency periodic motion of the original system (equations (4) and (5)).

In the non-resonant case, the bifurcation equations are formally obtained from equations (21) and (22) by omitting terms in $\exp(\pm i\,\Delta t_2)$. This procedure leads to the following four equations:

$$\begin{cases} \dot{a}_1 = \nu R_{11}a_1 + R_{12}a_1^3 + R_{13}a_1a_2^2 \\ \dot{a}_2 = \nu R_{24}a_2 + R_{25}a_2^3 + R_{26}a_2a_1^2 \end{cases} \tag{27a}$$

$$\begin{cases} a_1\dot{\varphi}_1 = a_1(\nu I_{11} + I_{12}a_1^2 + I_{13}a_2^2) \\ a_2\dot{\varphi}_2 = a_2(\nu I_{24} + I_{25}a_2^2 + I_{26}a_1^2). \end{cases} \tag{27b}$$

In equations (27) amplitude modulation equations (27a) are uncoupled from the phase modulation equations (27b) and can be studied by portrait phase techniques. Steady-state solutions of

the equations (27a) are determined by setting $\dot{a}_1 = \dot{a}_2 = 0$. The fixed points of the equation (27a) correspond to one-frequency periodic motion ($a_1 \neq 0, a_2 = 0$) and ($a_1 = 0, a_2 \neq 0$) or two-frequency quasi-periodic motions ($a_1 \neq 0, a_2 \neq 0$) of the original system (equations (4) and (5)).

Equations (27) are identical to those obtained in [10] and they are also identical to equations in standard normal form obtained by means of Center Manifold Theory [11]. In particular they are formally identical to double pendulum equations presented in [11] but with a lower codimension. This implies that, only one scenario of phase portrait exists for any $\nu > 0$. In any case, from [11] it is deduced that non-resonant two-component solutions are always unstable.

Finally, the case in which a simple Hopf bifurcation occurs at the point **O** it is still obtained from nearly-resonant equations. For example, by letting $a_2 = \varphi_2 = 0$ and $a_1 = a, \varphi_1 = \varphi$ in equations (27), the standard normal form of the simple Hopf bifurcation equations is drawn:

$$\dot{a} = \nu R_{11} a + R_{12} a^3 \qquad a\dot{\varphi} = a(\nu I_{11} + I_{12} a^2), \tag{28}$$

where a and φ are amplitude and phase of the periodic bifurcated solution. These amplitude equations are identical to those obtained in [13] for a simple Hopf bifurcation of a generic system.

Therefore, the proposed amplitude modulation equations (21) and (22) are comprehensive of all particular cases (simple and double, non-resonant and nearly-resonant Hopf bifurcations) except in the case of nilpotent critical Jacobian matrix ($\Delta = 0$).

In order to check the fitting between resonant and non-resonant solutions it is necessary to analyze the asymptotic behavior of the nearly-resonant amplitude equations (24–26) when the detuning Δ becomes large, i.e. when the ordering (20) is violated. In such a case, if the amplitudes a_1 and a_2 are of the same order, the last term of equation (26) dominates the remaining ones and cannot be balanced. Therefore $\dot{\gamma} = 0$ entails $a_1 \ll a_2$ or $a_2 \ll a_1$, i.e. weakly coupled bi-modal steady-state solutions. For example, by letting $a_1 \to 0$ in equations (24–26), equation (25) tends to the corresponding non-resonant equation ($27a_2$), from which a_2 is drawn, whereas the remaining two equations furnish the other two unknowns. Thus, one-frequency non-resonant periodic solutions are (nearly) recovered. On the other hand, when $a_1 = O(a_2)$, from equation (26) it follows that $\gamma \simeq \gamma(0) + \Delta t$, so that equations (24) and (25) differ from the associated equations (27a) for the presence of high-frequency forcing-terms. Nearly-resonant solutions are therefore identical to non-resonant solutions apart from small high-frequency periodic perturbations. It should be noted that, due to such perturbations, two-frequencies quasi-periodic non-resonant motions are not recovered as fixed-points of the asymptotic form of equations (24–26). By comparing resonant and non-resonant solutions it is possible to check whether a system is actually resonant or not, and consequently to evaluate the width of the resonant region.

5. Numerical Results

The behavior of a string around a double Hopf bifurcation is analyzed. A cross-section with a particularly thick ice accretion shape which has appeared in the literature (NDT-modified, [6]), is considered, subjected to non-symmetric wind flow. In fact, by using equations (7), it is easy to check that if the flow is symmetric (i.e. modes are decoupled) simple Hopf bifurcations only may occur, since $\det \mathbf{C}_a < 0$. A taut string is considered with parameters $\alpha = 928.13$, $\beta = 0$, $L = 244\,\text{m}$, $m = 6.15$ Kg/m, $\xi = 0.44\,\%$, $H = 32.000$ N and $b = 0.09\,\text{m}$. The

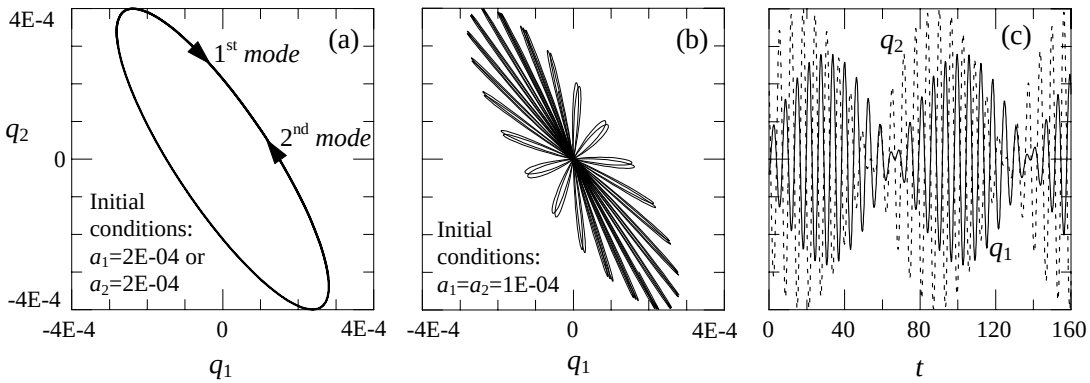

Figure 3. Linearized motion at criticality: (a) critical modes, (b) resultant motion, (c) time-history.

nonlinear aerodynamic coefficients are obtained from the available experimental data [14] by using natural cubic splines. The critical detuning Δ is equal to 0.0878. For this string a double Hopf bifurcation arises for critical wind velocity. In Figure 3(a) the first and second critical modes are shown in the configuration space. The two modes are complex with the same spatial shape described clockwise in the first mode, and counterclockwise in the second mode, with slightly different frequencies. Therefore, the resultant linearized motion is quasi-periodic (Figures 3(b), 3(c)) and possible bi-modal galloping takes place.

A nonlinear analysis is performed using both nearly-resonant and non-resonant solutions in the neighborhood of the bifurcation point (i.e. for small values of the control parameter ν). At the critical velocity μ_c ($V = 11.2$ m/s), fixed point branches with a typical galloping shape (e.g. see [5]) bifurcate from the trivial path (Figure 4). The stability of these branches has been verified by using standard methods (i.e. by analyzing eigenvalues of the Jacobian matrix). The non-resonant solution gives origin to three different branches (Figure 4(a)), two mono-modals and one bi-modal; the mono-modal solutions (solid lines, branches A and B) are always stable in the analyzed velocity field, whereas the bi-modal solution (dashed line, branch C) is always unstable. Figure 4(b) shows branches deriving from the nearly-resonant solution: branches A and B are practically identical to the previous ones, but with a very small coupled component; on the contrary, the bi-modal branch C is not found, according to the asymptotic behavior of equations (24–26) discussed in Section 4.

The previous results are corroborated by the analysis of transient motions, which are studied through direct numerical integration of the non-resonant (27) and nearly-resonant (24–26) amplitude equations. By considering the bifurcation as non-resonant, phase curves in the amplitude plane (a_1, a_2), originating from different initial conditions, are represented in Figure 5(a). Two stable mono-modal solutions (A, B) are found together with an unstable bi-modal solution (C, saddle point). Therefore, when the transient is exhausted, the cable oscillates in one mode only, similarly to a simple Hopf bifurcation. However, the initial conditions now determine which of them is the regime solution. In Figure 5(b) the problem is solved by using the nearly-resonant solution; the same initial conditions as in Figure 5(a) are imposed. A comparison between the two solutions reveals that the projection of the nearly-resonant phase curves (a_1, a_2, γ) on the modal amplitude plane (a_1, a_2) is wrapped around the non-resonant solution, with very small changes in the fixed point values. However, point C marked in Figure 5b is not a fixed point, as it has been discussed in Section 4. In fact, around point C, while the amplitudes a_1 and a_2

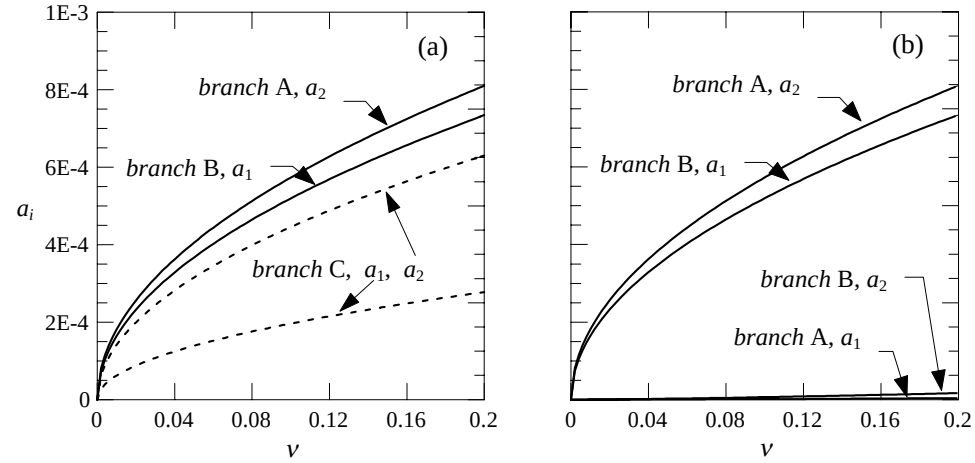

Figure 4. (a) Non-resonant and (b) nearly-resonant steady-state amplitude solution vs. adimensional wind velocity for the basic example.

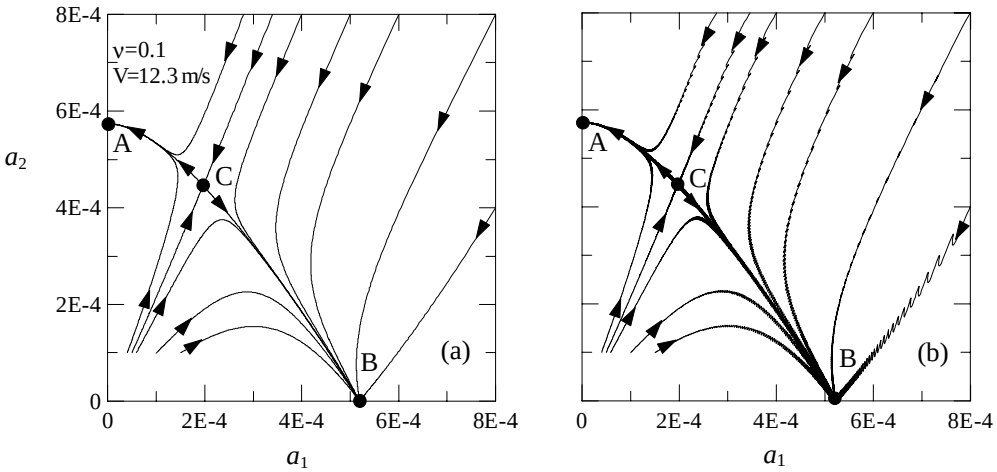

Figure 5. (a) Non-resonant and (b) nearly-resonant phase curves for the basic example.

remain nearly constant over an interval of time, the phase difference γ grows linearly in time. After that, the motion evolves toward a 'true' fixed point, A or B.

In conclusion, the system analyzed has to be considered as non-resonant. This implies that the resonant layer around the parabola of Figure 1 is very narrow.

In order to study the transition to the resonance, the basic example has been modified by progressively increasing the lift coefficient, therefore by reducing det $\mathbf{C}_a$ and leaving tr$\mathbf{C}_a$ unchanged. In this way a class of systems has been obtained, represented on the invariant plane (Figure 1) by points increasingly closer to the critical parabola. Correspondingly the following qualitative behavior of the fixed points on the amplitude plane has been observed. The unstable point C moves towards the stable point A until they coalesce and a bifurcation takes place. From this bifurcation a new unstable bi-modal point D arises. Meanwhile, simultaneously to the coalescence, point B moves away from the horizontal axis, remaining stable. It represents now a bi-modal galloping in which the in-plane and out-of-plane modal amplitudes are of the

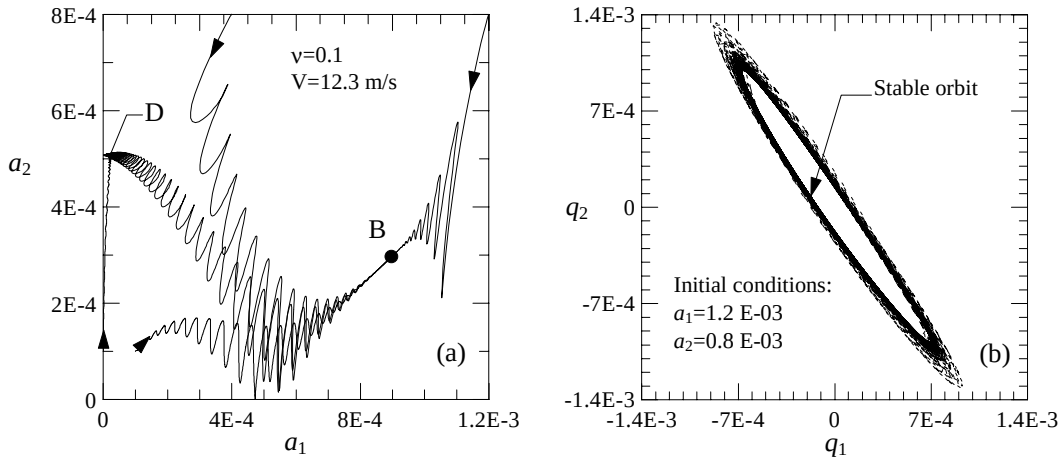

Figure 6. (a) Phase curves and (b) transient motion at the mid-span for the modified example.

same order. Therefore, the transition to the resonance is identified by the coalescence of fixed points C and A. The phase in which points C and A approach each other is well described by the non-resonant equations (27). These supply an estimate of the critical value of detuning which turns out to be independent of ν.

The modified example presented in Figure 6 is obtained by increasing the lift coefficient by about 15 %, corresponding to a detuning $\Delta = 0.0145$. By projecting the phases on the modal amplitude plane the phase portrait of Figure 6(a) follows. By perturbing the trivial equilibrium position along the vertical axis, the trajectory is first attracted by the unstable node D around which it remains for an interval of time; successively, the motion evolves towards the stable node B where a steady-state two-component oscillation takes place. The motion is periodic since in a nearly-resonant case, nonlinearities adjust the frequencies to match each other. Figure 6(b) presents the transient motion of the string mid-point for a second-order ε^2 approximation. The internal ellipse represents the stable bi-modal configuration (B), reached after transient oscillations (dot lines) of larger amplitude than those of the regime.

6. Conclusions and Remarks

Concerning taut strings subject to galloping, a complete classification of different critical conditions is given. By using the multiple scale perturbation method, nearly-resonant and non-resonant amplitude equations are drawn. The asymptotic behavior of the nearly-resonant equations when the detuning is large has been discussed and the transition between resonant and non-resonant solutions has been studied. When the system is non-resonant, two stable steady-state mono-modal solutions and one unstable bi-modal solution exist. When the system is nearly-resonant, two bi-modal solutions, one stable and the other unstable, appear. Hence, in both cases, when the transient is exhausted, the motion in the postcritical range is periodic. Therefore, linear quasi-periodic solutions, like those commented in [6], are disrupted by nonlinearities. Comparison of nearly-resonant and non-resonant solutions shows that the resonant region is very narrow. However, the magnitude of nonlinearities influence the resonant region. In the case treated here the thickness of the resonant layer strongly depends on the magnitude of nonlinear aerodynamic terms; the resonant region is wider when nonlinear aerodynamic terms are smaller

than those considered here. Therefore, it seems very important to possess reliable aerodynamic experimental data in order to obtain a correct estimation of the resonant region thickness.

Appendix A

The aerodynamic b_i and mechanical c_i coefficients of the discrete model (equations (4) and (5)) are:

$$
\begin{aligned}
b_1 &= 2\xi_1\omega_1 + \frac{\sqrt{\chi}}{\pi}c_d\mu, \quad b_2 = \frac{r_4}{r_{11}}\frac{\sqrt{\chi}}{2\pi}\left(c_d' - c_l\right)\mu, \quad b_3 = \frac{r_4}{r_5}\frac{\sqrt{\chi}}{\pi}c_l\mu,\\
b_4 &= 2\xi_2\omega_2 + \frac{\sqrt{\chi}}{2\pi}\left(c_d + c_l'\right)\mu, \quad b_5 = -\frac{r_{12}}{r_{11}}\frac{\eta}{2}c_d, \quad b_6 = -\frac{r_8}{r_{11}}\frac{\eta}{4}\left(c_d'' + c_d - 2c_l'\right),\\
b_7 &= -\frac{r_6}{r_{11}}\frac{\eta}{2}\left(c_d' - c_l\right), \quad b_8 = \frac{r_{13}}{r_{11}}\eta^2\frac{\pi}{12\sqrt{\chi}}\left(c_d''' + c_d' - 3c_l'' - 3c_l\right)\frac{1}{\mu},\\
b_9 &= -\frac{r_6}{r_5}\frac{\eta}{2}c_l, \quad b_{10} = -\frac{r_7}{r_5}\frac{\eta}{4}\left(c_l'' + c_l + 2c_d'\right), \quad b_{11} = -\frac{r_8}{r_5}\frac{\eta}{2}\left(c_d + c_l'\right),\\
b_{12} &= \frac{r_9}{r_5}\eta^2\frac{\pi}{12\sqrt{\chi}}\left(c_l''' + c_l' + 3c_d'' + 3c_d\right)\frac{1}{\mu}, \quad c_1 = -\frac{r_1 r_3}{r_{11}\pi^2}\alpha\beta,\\
c_2 &= \frac{r_3^2}{2r_{11}\pi^2}\alpha, \quad c_3 = \frac{r_2 r_3}{2r_{11}\pi^2}\alpha, \quad c_4 = -\frac{r_1 r_3}{2r_5\pi^2}\alpha\beta, \quad c_5 = -\frac{3r_1 r_2}{2r_5\pi^2}\alpha\beta,\\
c_6 &= \frac{r_2 r_3}{2r_5\pi^2}\alpha, \quad c_7 = \frac{r_2^2}{2r_5\pi^2}\alpha
\end{aligned}
$$

where ξ_i are the modal damping coefficients; c_j', c_j'', c_j''' $(j = d, l)$ are the first, second and third derivatives of drag (d) and lift (l) coefficients, with respect to the fluctuating angle of attack [5]; $\chi = mgL/H$ and $\eta = \rho bL/m$ are non-dimensional factors; ρ is the air density; b is the characteristic dimension of the cylinder cross-section (i.e. the cable diameter); r_i are the following modal terms:

$$
\begin{aligned}
r_1 &= \int_0^1 \phi_2 \mathrm{d}s, \quad r_2 = \int_0^1 \phi_2'^2 \mathrm{d}s, \quad r_3 = \int_0^1 \phi_1'^2 \mathrm{d}s, \quad r_4 = \int_0^1 \phi_1\phi_2 \mathrm{d}s,\\
r_5 &= \int_0^1 \phi_2^2 \mathrm{d}s, \quad r_6 = \int_0^1 \phi_1^2\phi_2 \mathrm{d}s, \quad r_7 = \int_0^1 \phi_2^3 \mathrm{d}s,\\
r_8 &= \int_0^1 \phi_1\phi_2^2 \mathrm{d}s, \quad r_9 = \int_0^1 \phi_2^4 \mathrm{d}s, \quad r_{10} = \int_0^1 \phi_1 \mathrm{d}s, \quad r_{11} = \int_0^1 \phi_1^2 \mathrm{d}s,\\
r_{12} &= \int_0^1 \phi_1^3 \mathrm{d}s, \quad r_{13} = \int_0^1 \phi_1\phi_2^3 \mathrm{d}s,
\end{aligned}
$$

where $\phi_1(s)$ and $\phi_2(s)$ are the linear vibration mode shapes [4]. In particular, the first linear symmetric modes for the string ($\beta = 0$) are $\phi_1(s) = \phi_2(s) = \sin(\pi s)$.

Appendix B

Coefficients appearing in solvability conditions (21) and (22) are defined as follows:

$$
\begin{aligned}
C_{j1} &= \mathbf{v}_j^H \mathbf{F}^0_{\mathbf{x}\nu}\mathbf{u}_1, \quad C_{j2} = \tfrac{1}{8}\mathbf{v}_j^H[\mathbf{F}^0_{\mathbf{xx}}(2\mathbf{u}_1\mathbf{z}_{1\bar{1}} + \mathbf{z}_{11}\bar{\mathbf{u}}_1) + \mathbf{F}^0_{\mathbf{xxx}}\mathbf{u}_1^2\bar{\mathbf{u}}_1] \\
C_{j3} &= \tfrac{1}{4}\mathbf{v}_j^H[\mathbf{F}^0_{\mathbf{xx}}(\mathbf{u}_1\mathbf{z}_{2\bar{2}} + \mathbf{u}_2\mathbf{z}_{1\bar{2}} + \mathbf{z}_{12}\bar{\mathbf{u}}_2) + \mathbf{F}^0_{\mathbf{xxx}}\mathbf{u}_1\mathbf{u}_2\bar{\mathbf{u}}_2] \\
C_{j4} &= \mathbf{v}_j^H \mathbf{F}^0_{\mathbf{x}\nu}\mathbf{u}_2, \quad C_{j5} = \tfrac{1}{8}\mathbf{v}_j^H[\mathbf{F}^0_{\mathbf{xx}}(2\mathbf{u}_2\mathbf{z}_{2\bar{2}} + \mathbf{z}_{22}\bar{\mathbf{u}}_2) + \mathbf{F}^0_{\mathbf{xxx}}\mathbf{u}_2^2\bar{\mathbf{u}}_2] \\
C_{j6} &= \tfrac{1}{4}\mathbf{v}_j^H[\mathbf{F}^0_{\mathbf{xx}}(\mathbf{u}_2\mathbf{z}_{1\bar{1}} + \mathbf{u}_1\mathbf{z}_{\bar{1}2} + \mathbf{z}_{12}\bar{\mathbf{u}}_1) + \mathbf{F}^0_{\mathbf{xxx}}\mathbf{u}_1\bar{\mathbf{u}}_1\mathbf{u}_2] \\
C_{j7} &= \tfrac{1}{8}\mathbf{v}_j^H[\mathbf{F}^0_{\mathbf{xx}}(2\mathbf{u}_1\mathbf{z}_{1\bar{2}} + \bar{\mathbf{u}}_2\mathbf{z}_{11}) + \mathbf{F}^0_{\mathbf{xxx}}\mathbf{u}_1^2\bar{\mathbf{u}}_2] \\
C_{j8} &= \tfrac{1}{8}\mathbf{v}_j^H[\mathbf{F}^0_{\mathbf{xx}}(2\mathbf{u}_2\mathbf{z}_{\bar{1}2} + \bar{\mathbf{u}}_1\mathbf{z}_{22}) + \mathbf{F}^0_{\mathbf{xxx}}\mathbf{u}_2^2\bar{\mathbf{u}}_1],
\end{aligned}
$$

where $(\ )^H$ denotes the transpose conjugate and $\mathbf{v}_j$ $(j = 1, 2)$ is the left eigenvector of the Jacobian matrix $\mathbf{F}^0_{\mathbf{x}}$ associated with the critical eigenvalue ω_{j0}. Right and left eigenvectors are assumed to be orthonormal in equations (21) and (22), i.e. $\mathbf{v}_i^H\mathbf{u}_j = \delta_{ij}$ where δ_{ij} is the Kronecker symbol.

References

1. Blevins, R.D., *Flow-induced Vibration*, 2nd edn, Van Nostrand Reinhold, New York, 1990.
2. Yu, P., Desai, Y.M., Shah, A.H., Popplewell., 'Three-degree-of-freedom model for galloping. Part I: Formulation and Part II: Solutions', *J. Eng. Mech.*, ASCE **119** (1993) 2404–2448.
3. Luongo, A., Rega, G., Vestroni, F., 'Planar non-linear free vibrations of an elastic cable', *Int. J. Non-Linear Mech.* **19** (1984) 39–52.
4. Lee, C.L., Perkins, N.C., 'Nonlinear oscillations of suspended cables containing a two-to-one internal resonance', *Nonlinear Dynamics* **3** (1992) 465–490.
5. Luongo, A., Piccardo, G., 'Non-linear galloping of iced suspended cables with two-to-one internal resonance', In: *Proc. Int. Symp. on Cable Dynamics*, Liege, Belgium, 1995, pp. 157–164.
6. Jones, K., 'Coupled vertical and horizontal galloping', *J. Eng. Mech.*, ASCE **118** (1992) 92–107.
7. Piccardo, G., Luongo, A., 'Critical conditions of flexural coupled galloping', In: *Proc. XII Italian Conf. of Theor. Appl. Mech.*, Naples, Italy, **2** 1995, pp. 161–166 (in Italian).
8. Perkins, N.C., Mote, C.D., 'Three-dimensional vibration of travelling elastic cables', *J. Sound Vib.* **114** (1987) 325–340.
9. Luongo, A., Piccardo, G., 'On the influence of the torsional stiffness on non-linear galloping of suspended cables', In: *Proc. 2nd ENOC*, Prague, Czech Republic, 1, 1996, pp. 273–276.
10. Luongo, A., Paolone, A., 'Perturbation methods for bifurcation analysis from multiple nonresonant complex eigenvalues', *Nonlinear Dynamics* **14** (1997) 193–210.
11. Troger, H., Steindl, A., *Nonlinear Stability and Bifurcation Theory*, Springer, Wien, 1991.
12. Luongo, A., 'Free vibrations and sensitivity analysis of a defective two degree-of-freedom system', *AIAA Journal* **33** (1995) 120–127.
13. Smith, L.L., Morino, L., 'Stability analysis of nonlinear differential autonomous systems with applications to flutter', *AIAA Journal* **14** (1976) 333–341.
14. Novak, M., Davenport, A.G., Tanaka, H., 'Vibration of towers due to galloping of iced cables', *J. Eng. Mech.*, ASCE **104** (1978) 457–473.